

# The magnetic helicity density patterns from non-axisymmetric solar dynamo

Valery V. Pipin

Institute for Solar-Terrestrial Physics, PO Box 291, Lermontov st., 126a, Irkutsk, 664033, Russia

(Received xx; revised xx; accepted xx)

In the paper we study the helicity density patterns which can result from the emerging bipolar regions. Using the relevant dynamo model and the magnetic helicity conservation law we find that the helicity density pattern around the bipolar regions depends on the configuration of the ambient large-scale magnetic field, and in general they show the quadrupole distribution. The position of this pattern relative to the equator can depend on the tilt of the bipolar region. We compute the time-latitude diagrams of the helicity density evolution. The longitudinally averaged effect of the bipolar regions show two bands of sign for the density distribution in each hemisphere. Similar helicity density patterns are provided by the helicity density flux from the emerging bipolar regions subjected to the surface differential rotation. Examining effect of helicity fluxes from the bipolar regions on the large-scale dynamo we find that its effect to the dynamo saturation is negligible.

## 1. Introduction

The magnetic helicity conservation is often considered as one of the most important ingredient in the magnetic field generation on the Sun and other solar type stars (Brandenburg & Subramanian 2005; Blackman & Thomas 2015). It is also important for the magnetic activities in the solar atmosphere and corona (Mackay & Yeates 2012). The magnetic helicity characterizes the complexity of the magnetic field topology in the closed volume (Berger 1984). Observing the magnetic field on the surface we can deduce some local proxies of the helicity integral. The observational constraints of the solar dynamo models are related to the hemispheric helicity rules (Seehafer 1994; Pevtsov *et al.* 1994) and the magnetic helicity fluxes from the solar interior (Berger & Ruzmaikin 2000; Blackman & Brandenburg 2003). The hemispheric helicity rule (hereafter HHR) follows from the theoretical properties of the large-scale dynamo which we expect to be working in the solar interior. This rule states that the small-scale magnetic fields on the northern hemisphere have the negative twist (the right-hand coordinate system) and the opposite twist is in the southern hemisphere. In the dynamo theory the small scales include scale of the solar active regions and smaller ones. The helicity conservation constrains the helicity sign distribution over the spatial scales. The results of Pouquet *et al.* (1975) showed that in the turbulent dynamo processes we can expect that the twist of the large-scale magnetic field is opposite to the twist of the small-scale magnetic field. This property is also called the bi-helical dynamo.

The vector magnetic field observations make possible to deduce the information about the magnetic and current helicity density on the solar surface (Pevtsov *et al.* 1994; Bao & Zhang 1998; Zhang *et al.* 2010). In general, these proxies show the HHR for the small-scale magnetic field. The issues about the HHR of the large-scale magnetic field and the

bi-helical solar dynamo are still debatable (Brandenburg *et al.* 2017; Singh *et al.* 2018; Pipin *et al.* 2019).

However, the relevance of the local proxies, which are observed on the surface, as the proxies of the bi-helical magnetic fields generated by the dynamo processes in the depth of the convection zone can be questioned. On the surface some of the helical magnetic field configurations can be generated by means of other processes which are not readily related to the dynamo. For example, the emerging of the magnetic field on the surface and its interaction with the ambient magnetic field can produce the local helicity flux. Hawkes & Yeates (2019) showed one of such example, see Fig4c in their paper. They illustrated that the emerging bipolar region which interacts with the global magnetic field results to the local quadrupole helicity density flux pattern. Interesting that this effect drives the helicity density flux butterfly diagrams, which are satisfying the own HHR, see the Fig3c in their paper. Another kind of this effect was illustrated by Pipin *et al.* (2019) in their benchmark dynamo model. Here we elaborate on this example and study the effect of the emerging bipolar regions on the surface helicity density patterns. Note, on the solar surface the most magnetic activity is produced by the sunspots (Stenflo 2013). It was found that the emerging active regions can bias our conclusions about the helical properties of the dynamo inside the convection zone. The study is based on the numerical simulations of the nonaxisymmetric dynamo model, which was suggested recently by Pipin & Kosovichev (2018a). The next section describes the model.

## 2. Dynamo model

Evolution of the large-scale magnetic field in perfectly conductive media is described by the mean-field induction equation (Krause & Rädler 1980):

$$\partial_t \langle \mathbf{B} \rangle = \nabla \times (\mathcal{E} + \langle \mathbf{U} \rangle \times \langle \mathbf{B} \rangle) \quad (2.1)$$

where  $\mathcal{E} = \langle \mathbf{u} \times \mathbf{b} \rangle$  is the mean electromotive force;  $\mathbf{u}$  and  $\mathbf{b}$  are the turbulent fluctuating velocity and magnetic field respectively; and  $\langle \mathbf{U} \rangle$  and  $\langle \mathbf{B} \rangle$  are the mean velocity and magnetic field. Pipin & Kosovichev (2018a) suggested the minimal set of the dynamo equations to model the non-axisymmetric magnetic field evolution. In this model, similarly to Moss *et al.* (2008), we neglect the radial dependence of magnetic field, and assume that the radial gradient of angular velocity is greater than the latitudinal gradient. It is convenient to represent the vector  $\langle \mathbf{B} \rangle$  in terms of the axisymmetric and non-axisymmetric components as follows:

$$\langle \mathbf{B} \rangle = \bar{\mathbf{B}} + \tilde{\mathbf{B}} \quad (2.2)$$

$$\bar{\mathbf{B}} = \hat{\phi} B + \nabla \times (A \hat{\phi}) \quad (2.3)$$

$$\tilde{\mathbf{B}} = \nabla \times (\mathbf{r}T) + \nabla \times \nabla \times (\mathbf{r}S), \quad (2.4)$$

where  $\bar{\mathbf{B}}$  and  $\tilde{\mathbf{B}}$  are the axisymmetric and non-axisymmetric components;  $A$ ,  $B$ ,  $T$  and  $S$  are scalar functions representing the field components;  $\hat{\phi}$  is the azimuthal unit vector,  $\mathbf{r}$  is the radius vector;  $r$  is the radial distance, and  $\theta$  is the polar angle. Hereafter, the over-bar denotes the axisymmetric magnetic field, and tilde denotes non-axisymmetric properties. Following the above ideas we consider a reduced dynamo model where we neglect the radial dependence of the magnetic field. In this case, the induction vector of the large-scale magnetic field is represented in terms of the scalar functions as follows:

$$\langle \mathbf{B} \rangle = -\frac{\mathbf{r}}{R^2} \frac{\partial \sin \theta A}{\partial \mu} - \frac{\hat{\theta}}{R} A + \hat{\phi} B \quad (2.5)$$

$$-\frac{\mathbf{r}}{R^2} \Delta_{\Omega} S + \frac{\hat{\theta}}{\sin \theta} \frac{\partial T}{\partial \phi} + \hat{\phi} \sin \theta \frac{\partial T}{\partial \mu},$$

where  $R$  represents the radius of the spherical surface inside a star where the hydromagnetic dynamo operates. The above equation defines the 3d divergency free B-field on the sphere. In the model we employ the simple expression of  $\mathcal{E}$ :

$$\mathcal{E} = \alpha \langle \mathbf{B} \rangle - \eta_T \nabla \times \langle \mathbf{B} \rangle + V_{\beta} \hat{\mathbf{r}} \times \mathbf{B} + \alpha_{\beta} \hat{\phi} \tilde{\mathbf{B}}_{\phi}. \quad (2.6)$$

The last term is introduced to simulated the tilt of the emerging active regions. The magnetic buoyancy is source of the non-axisymmetric magnetic field in the model. We assume that the magnetic buoyancy acts on relatively small-scale parts of the axisymmetric magnetic field, perhaps, it is caused by some kind of nonlinear instability. It is formulated as following:

$$V_{\beta} = \frac{\alpha_{MLT} u'}{\gamma} \beta^2 K(\beta) [1 + \xi_{\beta}(\phi, \theta)], \beta \geq \beta_{cr}, \quad (2.7)$$

and  $V_{\beta} = 0$  if  $\beta < \beta_{cr}$ , where  $\beta = |\langle \mathbf{B} \rangle| / B_{eq}$ ,  $B_{eq} = \sqrt{4\pi \bar{\rho} u'^2}$ , function  $K(\beta)$  is defined in Kitchatinov & Pipin (1993), function  $\xi_{\beta}(\phi, \theta)$  describes the latitudinal and longitudinal dependence of the instability, and parameter  $\beta_{cr}$  controls the instability threshold. In this formulation, the preferable latitude of the “active region emergence” is determined by the latitude of the maximum of the toroidal magnetic field energy,  $\theta_{max}$ . The magnetic buoyancy instability perturbations are determined by function:

$$\xi_{\beta}(\phi, \theta) = C_{\beta} \exp \left( -m_{\beta} \left( \sin^2 \left( \frac{\phi - \phi_0}{2} \right) + \sin^2 \left( \frac{\theta - \theta_{max}}{2} \right) \right) \right), \quad (2.8)$$

where  $m_{\beta} = 100$  controls the size of bipoles. The instability is randomly initiated in the northern or southern hemispheres, and the longitude,  $\phi_0$ , is also chosen randomly. In the model the strength of the magnetic field is measured relative to the strength of the equi-partition field,  $B_{eq}$ . Putting the parameter  $\beta_{cr} = 0.5$  we prevent emergence of active regions at high latitudes. The dynamic of the buoyancy instability is restricted by the five time run-steps. In the model we measure the time in the diffusive units,  $R^2/\eta_T$ . If we scale the dynamo period of the model to 11 years, then the simulated emerging time is about one week, which is much longer than on the Sun (Toriumi & Wang 2019). To get the model closer to observations the temporal and spatial resolution have to be increased. Bearing in mind the whole simplicity of our model we restrict ourselves to the qualitative considerations. We assume that the emerging part of the toroidal magnetic field is subjected to some extra  $\alpha$  effect, which is caused by the dynamic of the magnetic loop. We find that the  $5^{\circ}$  tilt (Tlatov *et al.* 2013) can be reproduced if we put

$$\alpha_{\beta} = \frac{1}{3} V_{\beta}, \quad (2.9)$$

where  $V_{\beta}$  is determined by the Eq(2.7). In case of  $\alpha_{\beta} = V_{\beta}$  the tilt is around  $\pi/4$ .

For the standard part of  $\alpha$  effect we use the isotropic expression and take into account the contribution of the magnetic helicity:

$$\alpha = \alpha_0 \cos \theta + \frac{\langle \chi \rangle \tau_c}{4\pi \bar{\rho} \ell^2} \quad (2.10)$$

where  $\alpha_0$  is a free parameter which controls the strength of the  $\alpha$ - effect, the second part of the Eq(2.10) expresses the effect of the magnetic helicity  $\langle \chi \rangle = \langle \mathbf{a} \cdot \mathbf{b} \rangle$  ( $\mathbf{a}$  and  $\mathbf{b}$  are the fluctuating parts of magnetic field vector-potential and magnetic field vector).

The magnetic helicity conservation results to the dynamical quenching of the dynamo. Contribution of the magnetic helicity to the  $\alpha$ -effect is expressed by the second term in Eq.(2.10). The magnetic helicity density of turbulent field,  $\langle \chi \rangle = \langle \mathbf{a} \cdot \mathbf{b} \rangle$ , is governed by the conservation law (Hubbard & Brandenburg 2012; Pipin *et al.* 2013; Brandenburg 2018):

$$\frac{\partial \langle \chi \rangle^{(tot)}}{\partial t} = -\frac{\langle \chi \rangle}{R_m \tau_c} - 2\eta \langle \mathbf{B} \rangle \cdot \langle \mathbf{J} \rangle - \nabla \cdot \mathcal{F}^\chi, \quad (2.11)$$

where  $\langle \chi \rangle^{(tot)} = \langle \chi \rangle + \langle \mathbf{A} \rangle \cdot \langle \mathbf{B} \rangle$  is the total magnetic helicity density of the mean and turbulent fields,  $\mathcal{F}^\chi = -\eta_\chi \nabla \langle \chi \rangle$  is the diffusive flux of the turbulent magnetic helicity, and  $R_m$  is the magnetic Reynolds number. The coefficient of the turbulent helicity diffusivity,  $\eta_\chi$ , is chosen ten times smaller than the isotropic part of the magnetic diffusivity (Mitra *et al.* 2010):  $\eta_\chi = \frac{1}{10} \eta_T$ . Similarly to the magnetic field, the mean magnetic helicity density can be formally decomposed into the axisymmetric and non-axisymmetric parts:  $\langle \chi \rangle^{(tot)} = \bar{\chi}^{(tot)} + \tilde{\chi}^{(tot)}$ . The same can be done for the magnetic helicity density of the turbulent field:  $\langle \chi \rangle = \bar{\chi} + \tilde{\chi}$ , where  $\bar{\chi} = \overline{\mathbf{a} \cdot \mathbf{b}}$  and  $\tilde{\chi} = \langle \mathbf{a} \cdot \tilde{\mathbf{b}} \rangle$ . Then we have,

$$\bar{\chi}^{(tot)} = \bar{\chi} + \overline{\mathbf{A}} \cdot \overline{\mathbf{B}} + \overline{\tilde{\mathbf{A}} \cdot \tilde{\mathbf{B}}}, \quad (2.12)$$

$$\tilde{\chi}^{(tot)} = \tilde{\chi} + \overline{\mathbf{A}} \cdot \tilde{\mathbf{B}} + \tilde{\mathbf{A}} \cdot \overline{\mathbf{B}} + \tilde{\mathbf{A}} \cdot \tilde{\mathbf{B}}, \quad (2.13)$$

Evolution of the  $\bar{\chi}$  and  $\tilde{\chi}$  is governed by the corresponding parts of Eq(2.11). Thus, the model takes into account contributions of the axisymmetric and nonaxisymmetric magnetic fields in the whole magnetic helicity density balance, providing a non-linear coupling. We see that the  $\alpha$ -effect is dynamically linked to the longitudinally averaged magnetic helicity of the  $\tilde{\mathbf{B}}$ -field, which is the last term in Eq(2.12). Thus, the nonlinear  $\alpha$ -effect is *non-axisymmetric*, and it contributes into coupling between the  $\overline{\mathbf{B}}$  and  $\tilde{\mathbf{B}}$  modes. The coupling works in both directions. For instance, the azimuthal  $\alpha$ -effect results in  $\mathcal{E}_\phi = \alpha \langle B_\phi \rangle + \alpha_\beta \tilde{B}_\phi$ . If we denote the nonaxisymmetric part of the  $\alpha$  by  $\tilde{\alpha}$  then the mean electromotive force is  $\bar{\mathcal{E}}_\phi = \bar{\alpha} \overline{B_\phi} + \tilde{\alpha} \tilde{B}_\phi + \alpha_\beta \tilde{B}_\phi$ . This introduces a new generation source which is usually ignored in the axisymmetric dynamo models. The magnetic helicity conservation is determined by the magnetic Reynolds number  $R_m$ . In this paper we employ  $R_m = 10^6$ .

The helicity conservation in form the Eq.(2.11) is suitable for the dynamo simulation. To estimate the helicity flux from the dynamo we will use the approach of Berger & Ruzmaikin (2000). Following their consideration the change of the helicity integral is determined by the the dynamo processes inside and the helicity fluxes out of the dynamo regions as follows

$$\frac{d}{dt} \int \langle \chi \rangle^{(tot)} dV = -2 \int \mathbf{E} \cdot \langle \mathbf{B} \rangle dV + \oint (\langle \mathbf{A} \rangle \times \mathbf{E}) \cdot \mathbf{ndS}, \quad (2.14)$$

where the electric field in perfectly conductive turbulent plasma, which is co-moving with mean flow  $\langle \mathbf{U} \rangle$ , is determined as follows,

$$\mathbf{E} = -\mathcal{E} - \langle \mathbf{U} \rangle \times \langle \mathbf{B} \rangle.$$

Note, that in our model we do not need to consider the relative helicity because we have the full information about the magnetic field and its potential from the dynamo evolution equation. Also, the integration volume in our case corresponds to thin spherical shell. The second term, i.e.,  $-\oint \langle \mathbf{A} \rangle \times \mathbf{E} dS$  describes the helicity fluxes out of the dynamo. The expression of the mean electromotive force contains contributions from the  $\alpha$ -effect,

turbulent diffusivity and the magnetic buoyancy. For this study we skip the effect of the turbulent diffusivity in  $\langle \mathbf{A} \rangle \times \mathbf{E}$  and we leave the  $\alpha$  and the magnetic buoyancy effects. Also we will estimate the effect of the differential rotation on the helicity flux to compare it with results of the earlier studies. Following the above comment we have:

$$\langle \langle \mathbf{A} \rangle \times \mathbf{E} \rangle \cdot \mathbf{n} = F_\Omega + F_\alpha + F_\beta + \dots, \quad (2.15)$$

$$F_\Omega = - \langle B_r \rangle \langle A_\phi \rangle \bar{U}_\phi, \quad (2.16)$$

$$F_\alpha = \alpha (\langle B_\theta \rangle \langle A_\phi \rangle - \langle B_\phi \rangle \langle A_\theta \rangle) - \alpha_\beta \tilde{B}_\phi \langle A_\theta \rangle \quad (2.17)$$

$$F_\beta = -V_\beta (\langle B_\theta \rangle \langle A_\theta \rangle - \langle B_\phi \rangle \langle A_\phi \rangle) \quad (2.18)$$

Note, that both the axisymmetric and the non-axisymmetric modes contribute to the all terms in Eq(2.15).

The equations (2.1,2.11) are solved numerically in the non-dimensional form. We assume that the rotational shear is constant in latitude. The effect of differential rotation is controlled by non-dimensional parameter  $R_\omega = \frac{R^2}{\eta_T} \frac{\partial \Omega}{\partial r}$ , the  $\alpha$ -effect is measured by parameter  $R_\alpha = \frac{R\bar{\alpha}}{\eta_T}$ , the magnetic buoyancy depends on  $R_\beta = \frac{R}{\eta_T} \frac{\alpha_{MLT} u'}{\gamma}$ , and the magnetic field is measured relative to the equipartition strength  $B_{eq} = \sqrt{4\pi\bar{\rho}u'^2}$ . Similarly to Pipin & Kosovichev (2018b) we put  $R_\omega = \frac{R\Omega}{\eta_T} = 10^3$ ,  $R_\alpha = 1$ . This choice describes the  $\alpha^2\Omega$  dynamo regime with differential rotation as the main driver of axisymmetric toroidal magnetic field. Note for the given choice of the dynamo parameters the non-axisymmetric modes are stable. They do not take part in the dynamo unless some non-axisymmetric phenomena come into the play. In this model the non-axisymmetric modes are resulted due to the magnetic buoyancy effect. To estimate the magnetic buoyancy parameter we employ results of (Kitchatinov & Pipin 1993) who argued that the maximum buoyancy velocity of large-scale magnetic field of equipartition strength  $B_{eq}$  is of the order of 6 m/s. In the solar conditions, the magnetic diffusion  $\eta_T = 10^{12} \text{cm}^2/\text{s}$  (Rüdiger *et al.* 2011), and  $R_\beta \approx 500$ . In our models, the large-scale magnetic field strength is below  $B_{eq}$ . Hence, we use by an order of magnitude smaller value:  $R_\beta = 50$ . In addition to nonlinear quenching of the  $\alpha$ -effect, the magnetic buoyancy also causes a nonlinear saturation of the dynamo process. Note, that the magnetic helicity in the model is measured in units  $B_{eq}^2 R$ . Comparing our results with observations, we have to bear in mind that in the model the magnetic field dynamo generation and the bipolar region formation occur in the same place. Therefore the resulted configuration of the axisymmetric magnetic field are expected to be different from the solar surface observation. However, the evolution of the non-axisymmetric magnetic field mimics the observational magnetic patterns reasonably well (see, Pipin & Kosovichev 2018b). The further detail about the model can be found in the above cited paper. Also, the python code for the model can be found at zenodo : Pipin (2018).

### 3. Results

#### 3.1. Helicity density patterns from bipolar regions

In this section we consider the helicity patterns, which are produced by the emerging bipolar regions. In this case, we start simulations with a simple antisymmetric distribution of the toroidal magnetic field,  $\bar{B}_\phi = \frac{1}{2} \sin 2\theta$ . The two bipolar regions are injected successively in the southern and northern hemispheres with interval about  $0.004R^2/\eta_T$ .

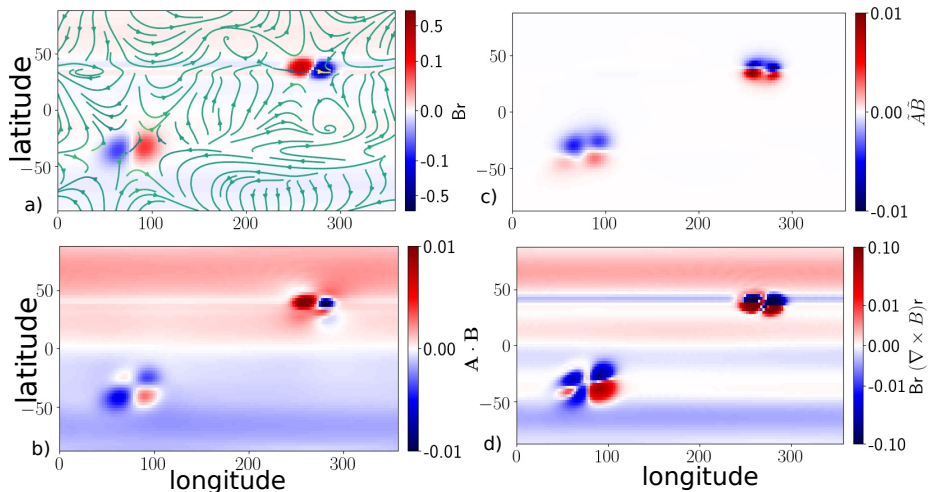


FIGURE 1. a) The color background shows the radial magnetic field (both the axisymmetric and the nonaxisymmetric modes), streamlines show the horizontal non-axisymmetric magnetic field; b) the total magnetic helicity density,  $(\bar{\mathbf{A}} + \tilde{\mathbf{A}}) \cdot (\bar{\mathbf{B}} + \tilde{\mathbf{B}})$ , c) the same as b) for  $\tilde{\mathbf{A}} \cdot \tilde{\mathbf{B}}$ ; d) the same as b) for the current helicity density.

The time in the model is measured in the units of the diffusive time. If we scale the dynamo period of the model to 11 years, then the interval  $0.004R^2/\eta_T$  corresponds to 2.5 months.

The Figure 1 illustrates the magnetic field configurations, as well as, the total helicity density,  $\bar{\mathbf{A}} \cdot \bar{\mathbf{B}} + \tilde{\mathbf{A}} \cdot \tilde{\mathbf{B}}$ , the helicity density of the nonaxisymmetric magnetic fields and the current helicity density distributions,  $B_r (\nabla \times \mathbf{B})_r$ . The snapshots are taken shortly after formation of the second bipolar region in the northern hemisphere. We see that the helicity density patterns of the bipolar regions have the quadrupole distributions. The large-scale helicity density is in the background. In agreement with the theoretical expectations, the large-scale magnetic field has the positive magnetic and current helicity density sign in the northern hemisphere. This helicity was generated by the large-scale dynamo. The emerging bipolar regions show the inverted quadrupole helicity patterns in the southern and the northern hemispheres. The positive and negative helicity density parts nearly cancel each other in each hemisphere. The effect of tilt most pronounced in distribution of the current helicity density. On the  $B_r (\nabla \times \mathbf{B})_r$  synoptic map we see the negative trace, which is produced by the emerging region. Therefore,  $\tilde{B}_r (\nabla \times \tilde{\mathbf{B}})_r < 0$  inside the latitudinal band of the bipolar region. We did not find this effect in another run where we neglect the  $\alpha_\beta$  term in the mean electromotive force. Also, some part of the net helicity is due to participation of the bipolar regions in the large-scale dynamo.

The Figure 2 illustrates the patterns of the helicity density fluxes, the terms,  $F_\Omega$ ,  $F_\alpha$  and  $F_\beta$  in the Eq(2.14) for the models with and without tilt effect. We find that coupling the emerging bipolar regions and the differential rotation produces the flux pattern which is inverted to the helicity density,  $\tilde{\mathbf{A}} \cdot \tilde{\mathbf{B}}$ . The Figures 2a) and d) agrees qualitatively with results of Hawkes & Yeates (2019) (see, Fig.4c, there). It is found that the fluxes  $F_\alpha$  and  $F_\beta$  are substantially smaller than the  $F_\Omega$ . Also, in all the cases the net helicity flux from each bipolar region is close to zero.

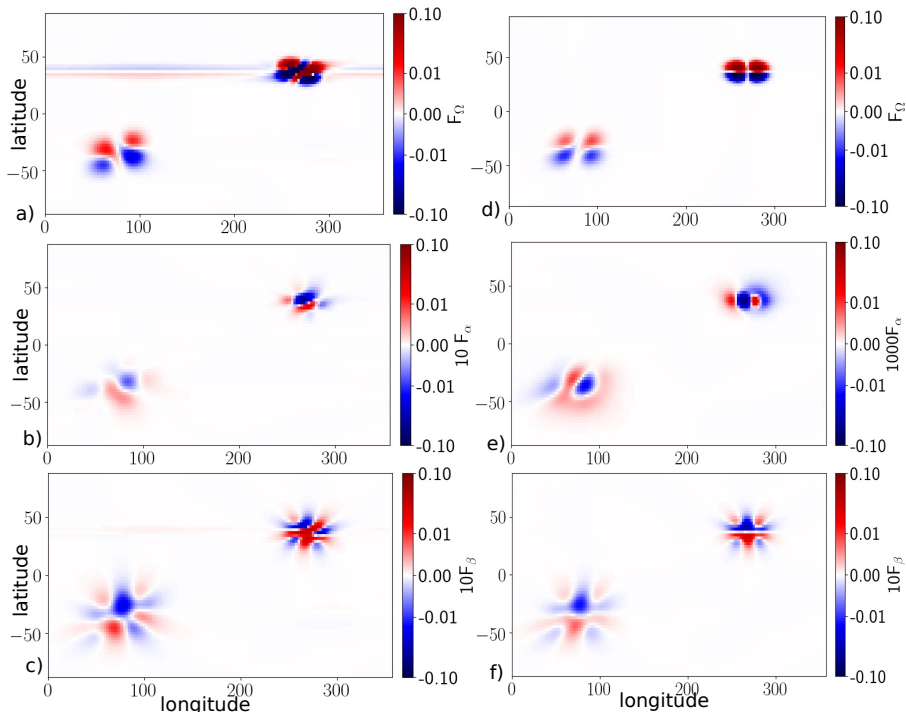


FIGURE 2. The helicity density fluxes, a)  $F_\Omega$  - the flux due to differential rotation; b) the flux due the  $\alpha$  - effect,  $F_\alpha$ ; c) the flux due to the magnetic buoyancy,  $F_\beta$ ; the panels d),e) and f) shows the same for the model without tilt, i.e.,  $\alpha_\beta = 0$ .

### 3.2. Bipolar regions in the dynamo evolution.

We make a run of the dynamo model with the random injections of the bipolar regions by means of the magnetic buoyancy instability. The instability is randomly initiated in the northern or southern hemispheres, and the longitude,  $\phi_0$ , is also chosen randomly. We arbitrary chose the fluctuation interval  $\tau_\beta = 0.01P$ . After injection of the perturbation the evolution is solely determined by the dynamo equations. Note, that the condition of the buoyancy instability is defined by the critical magnetic field strength, see the Eq.(2.7).

Figure shows the time-latitude diagrams for the toroidal magnetic field evolution, as well as , the small-scale helicity density,  $\bar{\chi}$  and the helicity density fluxe  $F_\Omega$ . In the model, the fluxes  $F_\alpha$  and  $F_\beta$  have less magnitude than the flux from the differential rotation and they, perhaps, do not present much interest. The model shows the regular dynamo waves of the toroidal magnetic field which drifts toward equator in course of the magnetic cycle. The emerging bipolar regions show no effect on the butterfly diagram because the coupling between axisymmetric and non-axisymmetric modes is weak. However, the bipolar regions have the cumulative effect on the rate of the magnetic flux loss. Therefore they affect the magnitude of the axisymmetric toroidal field. The properties of the given model was discussed in details by Pipin & Kosovichev (2018b). The small-scale helicity density,  $\bar{\chi}$  evolves in following conservation law helicity density. This conservation law preserves the integral balance between  $\bar{\chi}$ ,  $\overline{\mathbf{A} \cdot \mathbf{B}}$  and  $\overline{\mathbf{A}} \cdot \overline{\mathbf{B}}$ . In the quasi stationary state the  $\overline{\mathbf{A}} \cdot \overline{\mathbf{B}}$  contribution is much larger than  $\overline{\mathbf{A}} \cdot \overline{\mathbf{B}}$  (cf, Fig.4b). Therefore, the  $\bar{\chi}$  evolution follows the standard HHR. The time-latitude variations of the,  $\overline{\mathbf{A}} \cdot \overline{\mathbf{B}} = \bar{\chi}$ , show two bands in each hemisphere. The near equatorial bands show the positive sign in the northern

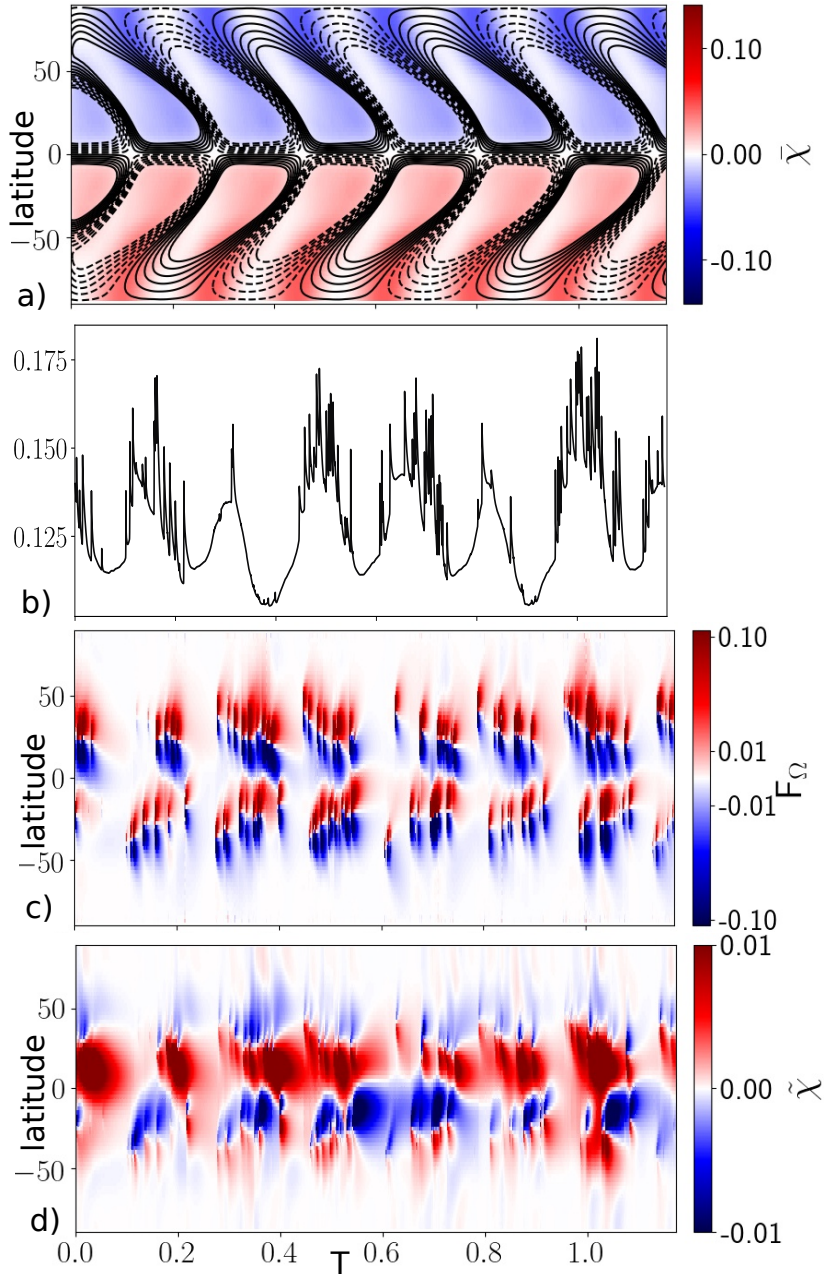


FIGURE 3. a) The time-latitude diagrams for the toroidal magnetic field (contours) and the small-scale helicity density,  $\bar{\chi}$ , is shown by the background image; b) the total flux of the radial magnetic field; c) the time-latitude diagram for the helicity flux from the differential rotations; d) the helicity density of the non-axisymmetric magnetic field.

hemisphere and the negative in the southern one. In the polar sides the situation is opposite. This patterns results naturally from the longitudinal averaging of the synoptic maps like that shown in Fig.1c. Interesting that in the run without tilt effect these bands show some equatorial drift, which results into noisy behavior of the  $\bar{\mathbf{A}} \cdot \bar{\mathbf{B}}$  near equator



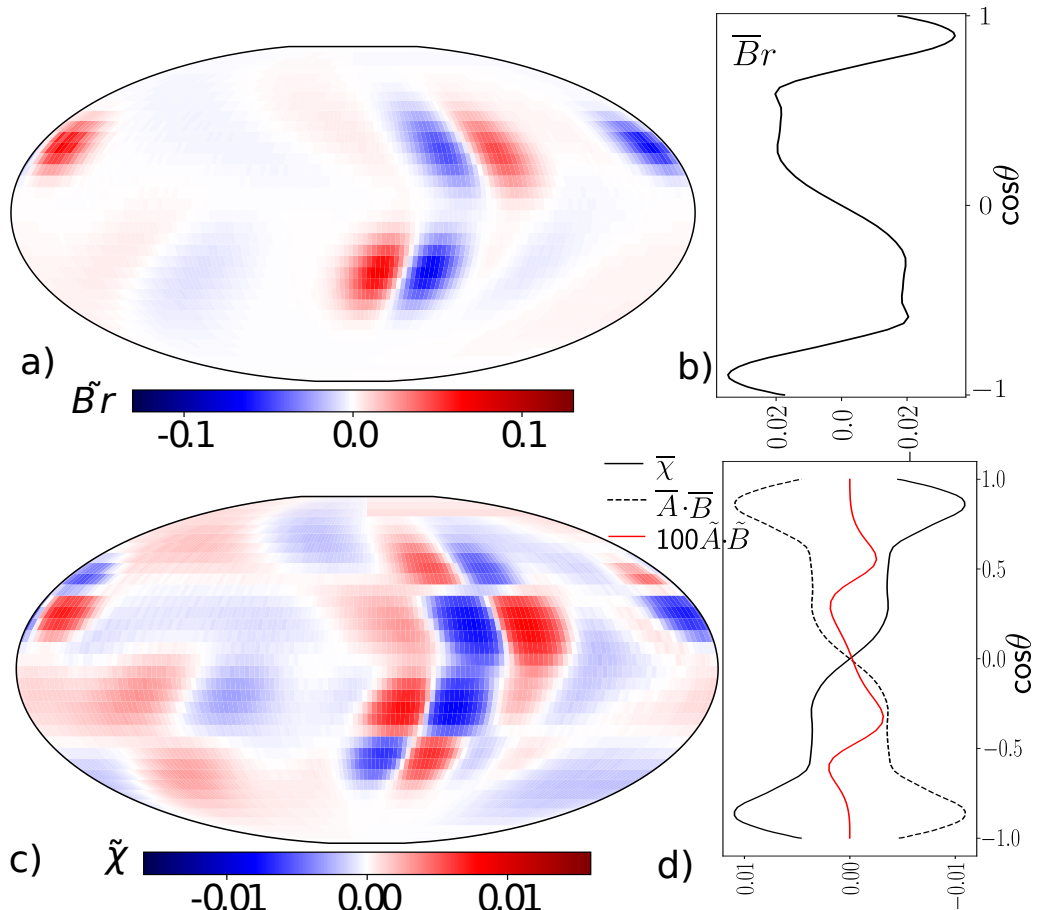


FIGURE 4. Snapshots of the magnetic field, (a), and the helicity density, (b), distributions for the maximum of the toroidal magnetic field cycle.

in that run. The time-latitude diagram of the  $\overline{\tilde{A} \cdot \tilde{B}}$  shows sometimes the same sign of helicity on both hemispheres. This period correspond to the time when the wave of the toroidal magnetic field goes close to equator. Therefore there is interaction of the bipolar regions emerging in opposite hemispheres. These periods correspond to local minima of the radial magnetic field flux. This parameter can be considered as a proxy of the sunspot activity (Stenflo 2013). For the  $F_\Omega$  the HHR tends to be opposite to the HHR of the non-axisymmetric magnetic field. The butterfly diagram of the  $F_\Omega$  agrees qualitatively with results of Hawkes & Yeates (2019) (see, Fig.3c, there). We also compute the time-latitude diagrams for the current helicity density,  $\overline{\tilde{B}_r (\nabla \times \tilde{\mathbf{B}})_r}$  and find that is similar to the  $\overline{\tilde{A} \cdot \tilde{B}}$ .

Figure 4 shows snapshots of the magnetic field and the helicity density distributions for the period of maximum of the toroidal magnetic field cycle. The helicity patterns near the bipolar regions are qualitatively similar to the case shown in Fig.1b and not in Fig.1c. Note, that the Fig.4b shows the helicity density of the non-axisymmetric magnetic field,  $\tilde{A} \cdot \tilde{B}$ . The interaction of the emerging bi-poles with the background large-scale non-axisymmetric magnetic field produces the pattern similar to that in Fig.1b. At the right side of the snapshot we show the mean distribution of the  $\overline{\chi}$ ,  $\overline{\tilde{A} \cdot \tilde{B}}$  and  $\overline{\tilde{A} \cdot \tilde{B}}$  for this

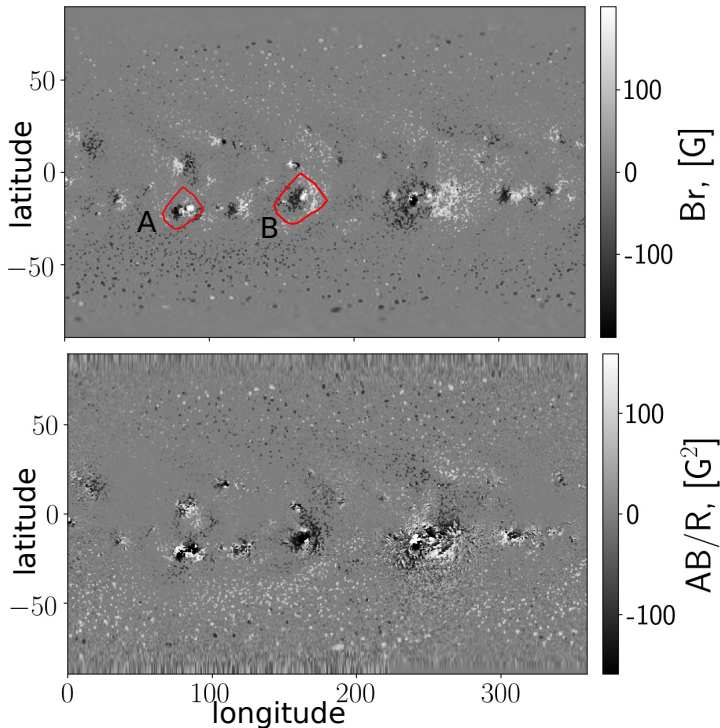


FIGURE 5. Synoptic maps of the radial magnetic field (top) and the magnetic helicity density (bottom) for the CR2157 (in following to results of Pipin *et al.* 2019).

synoptic map. We find that in the model the  $\overline{\tilde{\mathbf{A}} \cdot \tilde{\mathbf{B}}}$  has much less magnitude in compare with other two.

#### 4. Discussion and conclusions

In the paper we study the effect of the emerging bipolar regions on the magnetic helicity density distributions and the helicity density fluxes. Comparing our results with observations, we have to bear in mind that in the model the magnetic field dynamo generation and the bipolar region formation occur in the same place. Our main interest is to find some typical magnetic helicity pattern which we can observe on the surface of the Sun. We look to the case of the simple bipolar region which is formed from the large-scale toroidal magnetic field by means of the magnetic buoyancy. We find that such bipolar regions together with the large-scale magnetic field produce the quadrupole magnetic helicity density pattern (Figs1b,4c). The qualitatively similar helicity density patterns can be found in observations. Pipin *et al.* (2019) studied the helicity density distributions of the solar magnetic field using observations of the Helioseismic and Magnetic Imager (HMI, Scherrer *et al.* 2012) on board Solar Dynamics Observatory (SDO, Pesnell *et al.* 2012). The Figure 5 shows examples of the magnetic field and the magnetic helicity density synoptic maps for the Carrington rotation 2157. The two relatively small active regions in the southern hemisphere, A and B show the quaadrupole helicity density distributions in a qualitatively agreement with results of our study. The best agreement is for the region A. It is likely because it has a relatively simple distribution of the radial magnetic field flux.

In our model the dynamo process and the bipolar region formation occur in the same

place. In the large-scale dynamo, the emerging bipolar regions results into the loss of the magnetic field flux. This results into dynamo saturation. The effect of these bi-poles on the helical properties of the dynamo generated magnetic field is negligible. This is likely due to specific of the model. We find no considerable effect of the generated  $\overline{\tilde{\mathbf{A}} \cdot \tilde{\mathbf{B}}}$  on the small-scale helicity density evolution. The  $\overline{\tilde{\mathbf{A}} \cdot \tilde{\mathbf{B}}}$  shows the inverted HHR near equator in compare the sign of the current helicity density of the solar active regions, (Zhang *et al.* 2010, 2016). The positive sign of the magnetic helicity density from tilted bipolar regions was anticipated in earlier studies (Pevtsov *et al.* 2014). Moreover, it is expected the the tilted can get the internal twist opposing to the writhe by the magnetic tensions (Blackman & Brandenburg 2003). In our model this process is taken into account by the conservation law. Following to this law the small-scale helicity density  $\bar{\chi}$  evolves in balance with the  $\overline{\tilde{\mathbf{A}} \cdot \tilde{\mathbf{B}}}$  helicity density of the axisymmetric field,  $\overline{\mathbf{A}} \cdot \overline{\mathbf{B}}$ . The modeled  $\bar{\chi}$  distributions are determined by the axisymmetric type of the dynamo model.

Summing up, it is found the emerging bipolar regions produce the quadrupole helicity density patterns. The similar patterns were found for the helicity flux by means of the differential rotation. The model show no effect of the helicity evolution in the bipolar regions on the large-scale dynamo. We find that the tilted bipolar regions show the inverted hemispheric helicity rule near equator in compare with observations of the magnetic helicity in the solar active regions. In general, our results suggest that on the intermediate scales such as the scale of the bipolar active regions the averaged magnetic helicity distribution can show no definite sign distribution in the northern and southern hemisphere of the Sun.

**Acknowledgements** The author acknowledge the financial support by the Russian Foundation for Basic Research grant 19-52-53045 and support of scientific project FR II.16 of ISTP SB RAS. This work utilizes HMI data which are used here are courtesy of NASA/SDO and the HMI science teams. This work was borne out of discussions held among the authors during “Solar Helicities in Theory and Observations: Implications for Space Weather and Dynamo Theory” Program at Nordic Institute for Theoretical Physics (NORDITA) in 4–29 March 2019.

## REFERENCES

- BAO, S. & ZHANG, H. 1998 Patterns of current helicity for the twenty-second solar. *ApJ* **496**, L43–L46.
- BERGER, MITCHELL A.; FIELD, G. B. 1984 The topological properties of magnetic helicity. *Journal of Fluid Mechanics* **147**.
- BERGER, M. A. & RUZMAIKIN, A. 2000 Rate of helicity production by solar rotation. *J. Geophys. Res.* **105**, 10481–10490.
- BLACKMAN, E. G. & BRANDENBURG, A. 2003 Doubly helical coronal ejections from dynamos and their role in sustaining the solar cycle. *ApJL* **584**, L99–L102, arXiv: astro-ph/0212010.
- BLACKMAN, E. G. & THOMAS, J. H. 2015 Explaining the observed relation between stellar activity and rotation. *MNRAS* **446**, L51–L55, arXiv: 1407.8500.
- BRANDENBURG, A. 2018 Advances in mean-field dynamo theory and applications to astrophysical turbulence. *Journal of Plasma Physics* **84**, 735840404.
- BRANDENBURG, A., PETRIE, G. J. D. & SINGH, N. K. 2017 Two-scale analysis of solar magnetic helicity. *ApJ* **836**, 21.
- BRANDENBURG, A. & SUBRAMANIAN, K. 2005 Astrophysical magnetic fields and nonlinear dynamo theory. *Phys. Rep.* **417**, 1–209, arXiv: arXiv:astro-ph/0405052.
- HAWKES, G. & YEATES, A. R. 2019 Hemispheric injection of magnetic helicity by surface flux transport. *A & A* **631**, A138.
- HUBBARD, A. & BRANDENBURG, A. 2012 Catastrophic quenching in  $\alpha\Omega$  dynamos revisited. *ApJ* **748**, 51, arXiv: 1107.0238.

- KITCHATINOV, L. L. & PIPIN, V. V. 1993 Mean-field buoyancy. *A & A* **274**, 647–652.
- KRAUSE, F. & RÄDLER, K.-H. 1980 *Mean-Field Magnetohydrodynamics and Dynamo Theory*. Berlin: Akademie-Verlag.
- MACKAY, D. H. & YEATES, A. R. 2012 The sun's global photospheric and coronal magnetic fields: Observations and models. *Living Reviews in Solar Physics* **9**, 6, arXiv: 1211.6545.
- MITRA, D., CANDELARESI, S., CHATTERJEE, P., TAVAKOL, R. & BRANDENBURG, A. 2010 Equatorial magnetic helicity flux in simulations with different gauges. *Astronomische Nachrichten* **331**, 130, arXiv: 0911.0969.
- MOSS, D., SOKOLOFF, D., USOSKIN, I. & TUTUBALIN, V. 2008 Solar grand minima and random fluctuations in dynamo parameters. *Solar Phys.* **250**, 221–234.
- PESNELL, W. D., THOMPSON, B. J. & CHAMBERLIN, P. C. 2012 The solar dynamics observatory (sdo). *Sol.Phys.* **275**, 3–15.
- PEVTSOV, A. A., BERGER, M. A., NINDOS, A., NORTON, A. A. & VAN DRIEL-GESZTELYI, L. 2014 Magnetic helicity, tilt, and twist. *Space Sci. Rev.* **186**, 285–324.
- PEVTSOV, A. A., CANFIELD, R. C. & METCALF, T. R. 1994 Patterns of helicity in solar active regions. *ApJL* **425**, L117–L119.
- PIPIN, V. 2018 Vvpipin/2dspdy 0.1.1.
- PIPIN, V. V. & KOSOVICHEV, A. G. 2018a Does nonaxisymmetric dynamo operate in the sun? *ApJ* **867**, 145, arXiv: 1808.05332.
- PIPIN, V. V. & KOSOVICHEV, A. G. 2018b Does nonaxisymmetric dynamo operate in the sun? *ArXiv e-prints* p. arXiv:1808.05332, arXiv: 1808.05332.
- PIPIN, V. V., PEVTSOV, A. A., LIU, Y. & KOSOVICHEV, A. G. 2019 Evolution of magnetic helicity in solar cycle 24. *ApJ* **877** (2), L36, arXiv: 1905.00772.
- PIPIN, V. V., SOKOLOFF, D. D., ZHANG, H. & KUZANYAN, K. M. 2013 Helicity conservation in nonlinear mean-field solar dynamo. *ApJ* **768**, 46, arXiv: 1211.2420.
- POUQUET, A., FRISCH, U. & LÉORAT, J. 1975 Strong MHD helical turbulence and the nonlinear dynamo effect. *J. Fluid Mech.* **68**, 769–778.
- RÜDIGER, G., KITCHATINOV, L. L. & BRANDENBURG, A. 2011 Cross helicity and turbulent magnetic diffusivity in the solar convection zone. *Sol.Phys.* **269**, 3–12, arXiv: 1004.4881.
- SCHERRER, P. H., SCHOU, J., BUSH, R. I., KOSOVICHEV, A. G., BOGART, R. S., HOEKSEMA, J. T., LIU, Y., DUVAL, T. L., ZHAO, J., TITLE, A. M., SCHRIJVER, C. J., TARBELL, T. D. & TOMCZYK, S. 2012 The helioseismic and magnetic imager (hmi) investigation for the solar dynamics observatory (sdo). *Sol.Phys.* **275**, 207–227.
- SEEHAFER, N. 1994 Alpha effect in the solar atmosphere. *A & A* **284**, 593–598.
- SINGH, N. K., KÄPYLÄ, M. J., BRANDENBURG, A., KÄPYLÄ, PETRI, J., LAGG, A. & VIRTANEN, I. 2018 Bihelical spectrum of solar magnetic helicity and its evolution. *ApJ* **863**, 182, arXiv: 1804.04994.
- STENFLO, J. O. 2013 Solar magnetic fields as revealed by stokes polarimetry. *Astron. & Astrophys. Rev.* **21**, 66, arXiv: 1309.5454.
- TLATOV, A., ILLARIONOV, E., SOKOLOFF, D. & PIPIN, V. 2013 A new dynamo pattern revealed by the tilt angle of bipolar sunspot groups. *MNRAS* **432** (4), 2975–2984, arXiv: 1302.2715.
- TORIUMI, S. & WANG, H. 2019 Flare-productive active regions. *Living Reviews in Solar Physics* **16** (1), 3, arXiv: 1904.12027.
- ZHANG, H., BRANDENBURG, A. & SOKOLOFF, D. D. 2016 Evolution of magnetic helicity and energy spectra of solar active regions. *ApJ* **819**, 146.
- ZHANG, H., SAKURAI, T., PEVTSOV, A., GAO, Y., XU, H., SOKOLOFF, D. D. & KUZANYAN, K. 2010 A new dynamo pattern revealed by solar helical magnetic fields. *MNRAS* **402**, L30–L33, arXiv: 0911.5713.

## Appendix

Applying these simplifications to Eq (2.1) and Eqs (2.2-2.4) we obtain the following set of dynamo equations in terms of the scalar functions,  $A, B, S$ , and  $T$ :

$$\partial_t B = -\sin\theta \frac{\partial\Omega}{\partial r} \frac{\partial(\sin\theta A)}{\partial\mu} + \eta_T \frac{\sin^2\theta}{R^2} \frac{\partial^2(\sin\theta B)}{\partial\mu^2} \quad (4.1)$$

$$\begin{aligned}
& + \frac{\sin \theta}{R} \frac{\partial}{\partial \mu} \alpha \mu \langle B_r \rangle + \frac{\alpha \mu}{R} \langle B_\theta \rangle \\
& - \frac{1}{R} V_\beta \langle B_\phi \rangle - \frac{B}{\tau}
\end{aligned} \tag{4.2}$$

$$\partial_t A = \alpha \mu \langle B_\phi \rangle + \eta_T \frac{\sin^2 \theta}{R^2} \frac{\partial^2 (\sin \theta A)}{\partial \mu^2} - \frac{V_\beta}{R} A - \frac{A}{\tau}, \tag{4.3}$$

$$\partial_t \Delta_\Omega T = -\Delta_\Omega \delta \Omega \frac{\partial T}{\partial \phi} + \frac{\eta_T}{R^2} \Delta_\Omega^2 T \tag{4.4}$$

$$\begin{aligned}
& - \frac{1}{R} \frac{\partial \Omega}{\partial r} \sin^2 \theta \frac{\partial \Delta_\Omega S}{\partial \mu} - \frac{1}{R} \frac{\partial}{\partial \phi} \left[ \frac{\alpha + \alpha_\beta}{\sin \theta} \mu \langle B_\phi \rangle \right] \\
& + \Delta_\Omega \frac{\alpha \mu}{R} (\langle B_r \rangle \sin^2 \theta + \mu \sin \theta \langle B_\theta \rangle) \\
& + \frac{1}{R} \frac{\partial}{\partial \mu} \alpha \mu \sin \theta \{ \mu \sin \theta \langle B_r \rangle + \mu^2 \langle B_\theta \rangle \} \\
& - \frac{1}{R \sin \theta} \frac{\partial}{\partial \phi} \langle B_\theta \rangle V_\beta - \frac{\partial}{\partial \mu} (\sin \theta \langle B_\phi \rangle V_\beta),
\end{aligned} \tag{4.5}$$

$$\partial_t \Delta_\Omega S = - \left( \delta \Omega \Delta_\Omega \frac{\partial}{\partial \phi} S \right) + \frac{\eta_T}{R^2} \Delta_\Omega^2 S \tag{4.6}$$

$$\begin{aligned}
& + \frac{\partial}{\partial \mu} (\alpha + \alpha_\beta) \mu \sin \theta \langle B_\phi \rangle \\
& + \frac{\partial}{\partial \phi} \left\{ \frac{\alpha \mu}{\sin \theta} (\langle B_\theta \rangle + \sin \theta (\mathbf{e} \cdot \langle \mathbf{B} \rangle)) \right\} \\
& - \frac{1}{\sin \theta} \frac{\partial}{\partial \phi} (\langle B_\phi \rangle V_\beta) + \frac{\partial}{\partial \mu} (\sin \theta \langle B_\theta \rangle V_\beta),
\end{aligned} \tag{4.7}$$

where  $\Delta_\Omega = \frac{\partial}{\partial \mu} \sin^2 \theta \frac{\partial}{\partial \mu} + \frac{1}{\sin^2 \theta} \frac{\partial^2}{\partial \phi^2}$  and  $\mu = \cos \theta$ . To simulate stretching of non-axisymmetric magnetic field by the surface differential rotation we consider the latitudinal dependence of angular velocity  $\delta \Omega = -0.25 \sin^2 \theta \Omega$  in Eqs (4.4) and (4.6), which are written in the coordinate system rotating with angular velocity  $\Omega$ . The  $\tau$ -terms in Eqs(4.1,4.3) were suggested by Moss *et al.* (2008) to account for turbulent diffusion in radial direction. Similarly to the cited paper we put  $\tau = 3 \frac{R^2}{\eta_T}$ .